Temperature-driven phase transformations and microstructure evolution in the thermoelectric colusite $Cu_{26}V_2Sn_6S_{32}$. An *in situ* synchrotron diffraction study

F. Guiot[a], G. Guélou[b], C. Dejoie[c], A. Fitch[c], E. Guilmeau[b], K. Suekuni[d], P. Lemoine[e,*], C. Prestipino[b,**]

[a] *Univ. Rennes,, CNRS, ISCR-UMR 6226, F-35000 Rennes, France,*
[b] *CRISMAT, CNRS, Normandie Univ, ENSICAEN, Unicaen, 14000 Caen, France,*
[c] *ID22, Structure of Materials Group ESRF - The European Synchrotron, 38043 Grenoble, France,*
[d] *Graduate School of Advanced Sciences of Matter, Hiroshima University, Higashi-Hiroshima 739-8530, Japan,*
[e] *Université de Lorraine, CNRS, IJL, F-54000 Nancy, France,*

[*] pierric.lemoine@univ-lorraine.fr
[**] carmelo.prestipino@ensicaen.fr

1. Supplementary information

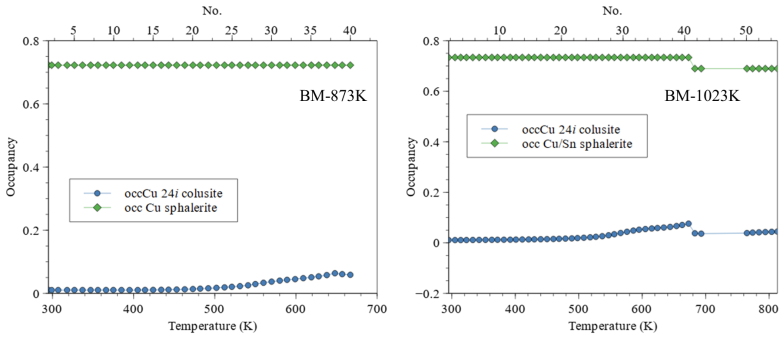

Figure S1: Thermal evolution of the occupation by copper atoms of the $24i$ site of colusite and $4a$ site of sphalerite-type phases for BM-873K (left) and BM-1023K (right) samples obtained by Rietveld refinement.

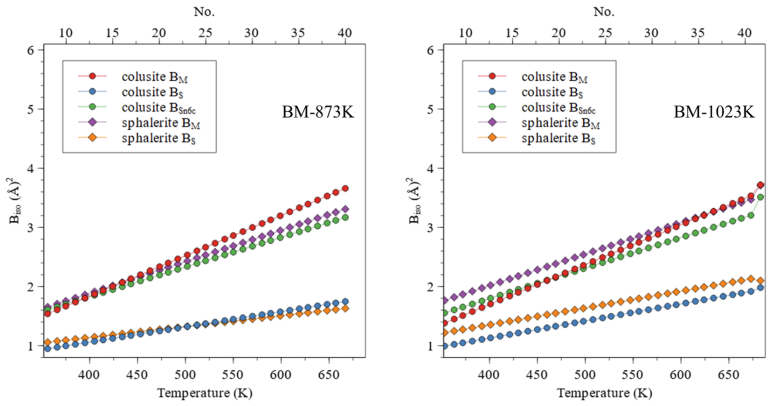

Figure S2: Thermal evolution of displacement factors Biso for BM-873K (left) and BM-1023K (right) samples obtained by Rietveld refinement.

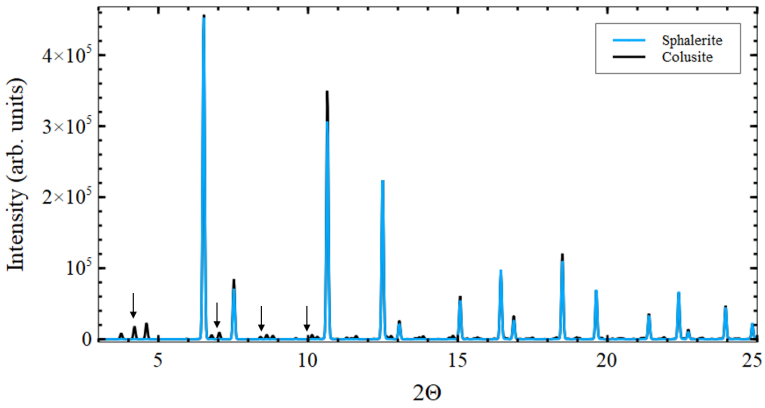

Figure S3: Simulated X-ray diffraction patterns of colusite and sphalerite. The black arrows represent the superstructure peaks of colusite satisfying $h+k$, $h+l$, $k+l = 2n+1$.

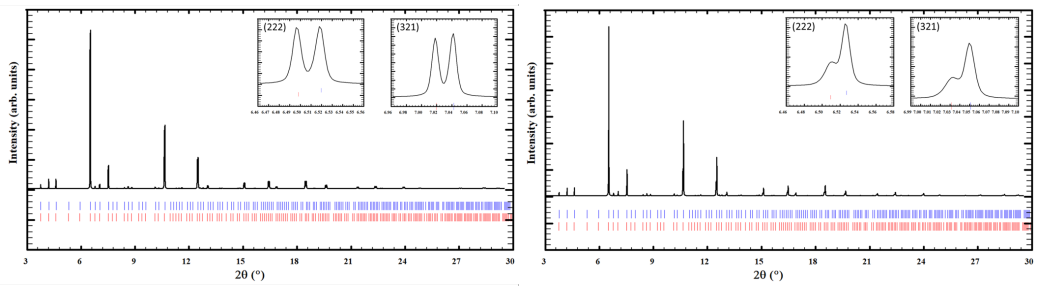

Figure S4: Simulation of synchrotron high resolution pattern of sample with (left) two colusite phases with high crystallinity, such as in sample BM-1023K, and (right) one colusite phase with high crystallinity and one colusite phase with poor crystallinity, such as in sample BM-873K. Insets show enlarged areas around (222) and (321) reflections referring to colusite structure.

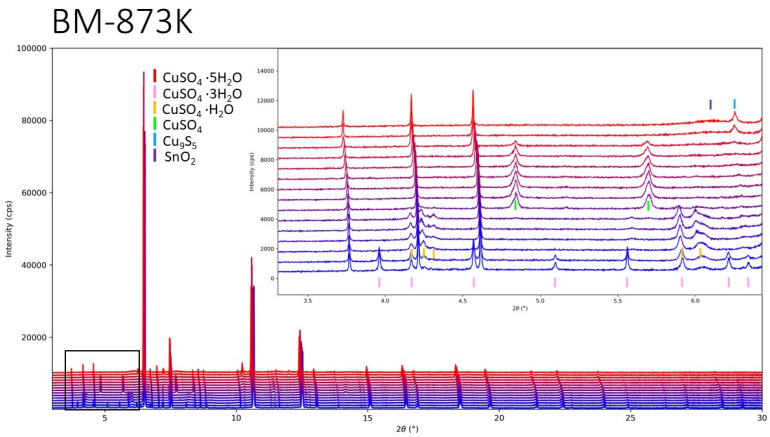

Figure S5: Evolution of the X-ray diffraction patterns for the BM-873K sample during the temperature ramp from RT to 667 K. The patterns are vertically offset and color-coded from blue to red with increasing temperature. For clarity, only one out of every three patterns is shown. The inset highlights the low-angle region (3–6°), emphasizing the sequential emergence and evolution of secondary phases and decomposition products. The peaks of secondary phases in the inset are indexed by colored ticks.

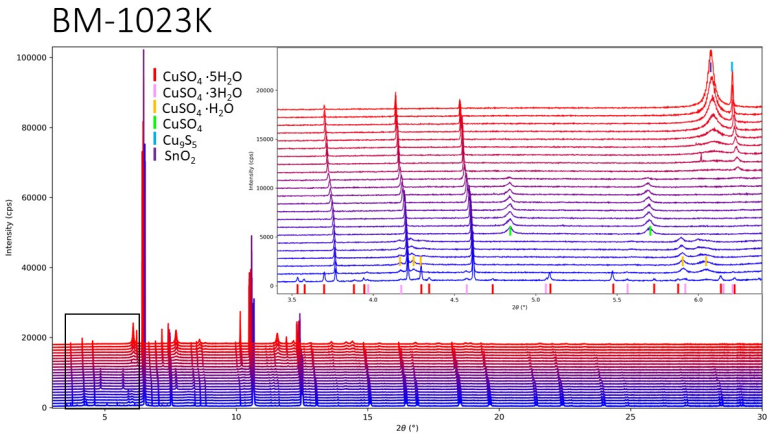

Figure S6: Evolution of the X-ray diffraction patterns for the BM-1023K sample during the temperature ramp from RT to 973 K. The patterns are vertically offset and color-coded from blue to red with increasing temperature. For clarity, only one out of every three patterns is shown. The inset highlights the low-angle region (3–6°), emphasizing the sequential emergence and evolution of secondary phases and decomposition products. The peaks of secondary phases in the inset are indexed by colored ticks.

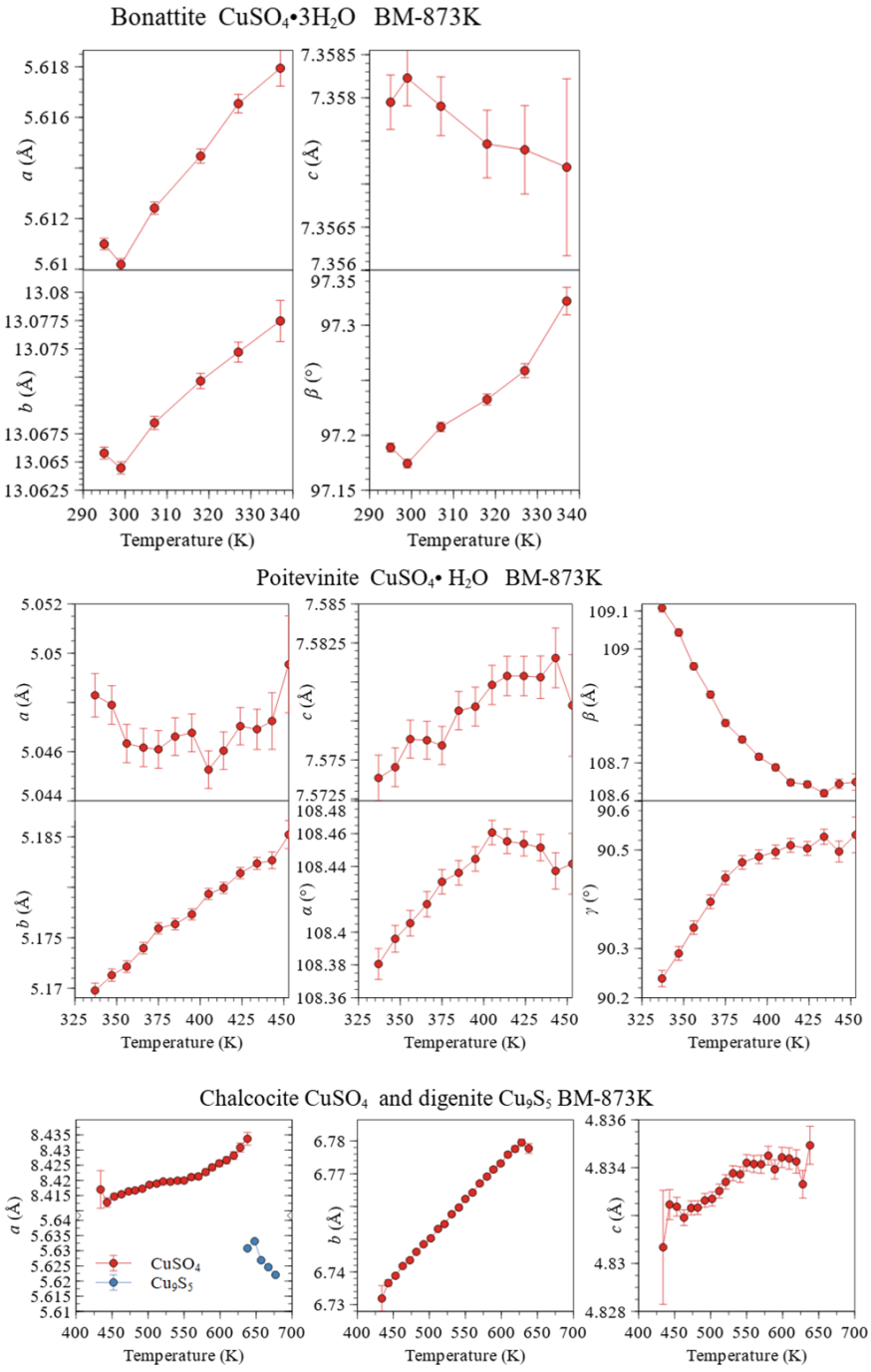

Figure S7: Cell parameters evolution of secondary phases as a function of the temperature for sample BM-873K.

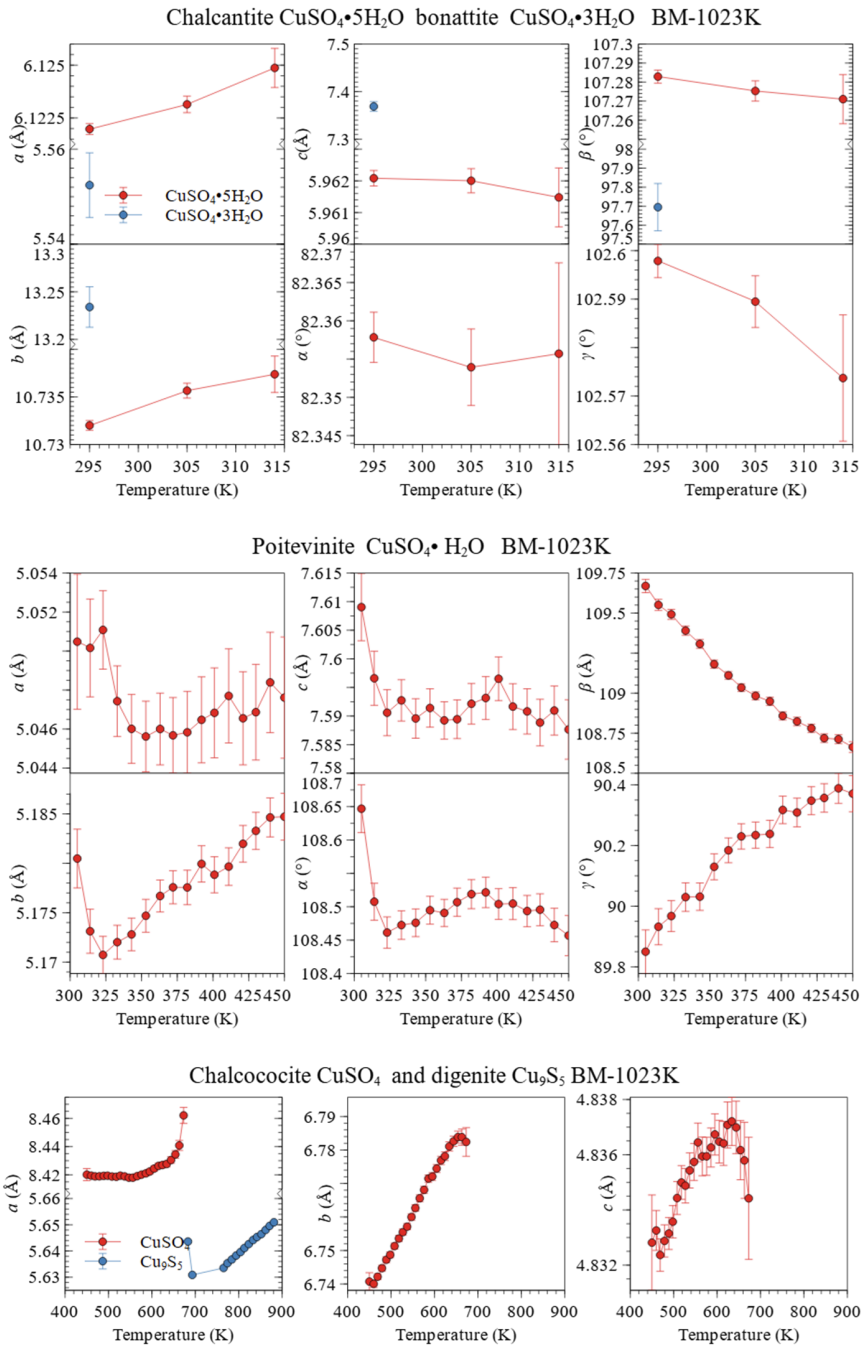

Figure S8: Cell parameters evolution of secondary phases as a function of the temperature for sample BM-1023K.

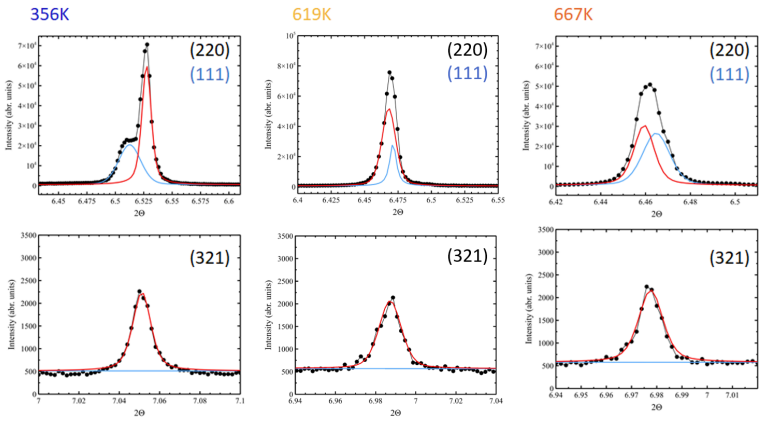

Figure S9: Enlarged views on selected Bragg peaks of Rietveld refinement of structural models (considering a colusite phase contribution in red and a sphalerite-type phase contribution in blue) against the XRPD patterns of $Cu_{26}V_2Sn_6S_{32}$ sample BM-873K recorded at 356 K, 619 K and 667 K (λ = 0.3542 Å).

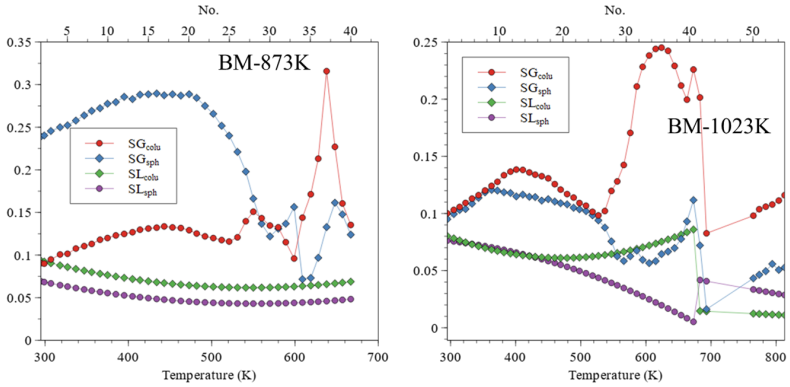

Figure S10: Thermal evolution of strain parameters for BM-873K (left) and BM-1023K (right) samples obtained by Rietveld refinement.

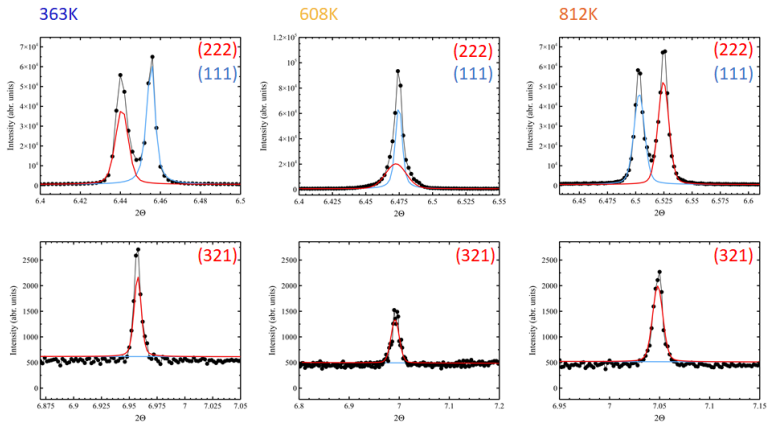

Figure S11: Enlarged views on selected Bragg peaks of Rietveld refinement of structural models (considering a colusite phase contribution in red and a sphalerite-type phase contribution in blue) against the XRPD patterns of $Cu_{26}V_2Sn_6S_{32}$ sample BM-1023K recorded at 363 K, 608 K and 812 K (λ = 0.3542 Å).

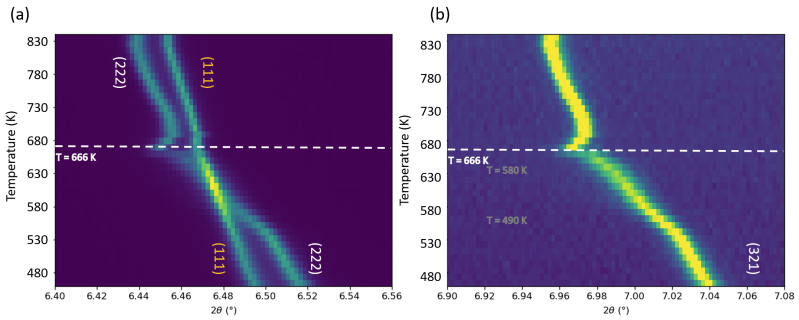

Figure S12: High-temperature XRPD thermograms of BM-1023K-2 sample recorded at the heating rate of 4 K min^{-1}. (a) Close-up view of the structure peak (222) of colusite and (111) of sphalerite, (b) superstructure peak (321) of the colusite phase.

Table S1: Resolution Function of ID22 obtained from LaB6 (λ = 0.336367 Å):

Profil	Shape 1	Shape 2	Shape 3
7	0.0	0.0	0.0
Lambda 1	Lambda 2	Ratio	
0.354246	0.354246	0.0	

Table S2: Geometry Type

GEOM SYNC	0.020000				
Th_{max}	Step	Th_{max}			
2.0	0.0010	60.0			
Asymmetry	S_L	S_D			
	0.027	0.013			
U-inst	V-inst	W-inst	X-inst	Y-inst	Z-inst
0.0	0.0	0.0	0.01719	0.00032	0.0

Table S3a: Crystal data and structure refinement for sample BM-873K

Parameter	**Cu-V-Sn-S (Colu)**	**Cu-Sn-S (sph)**
Crystal system	Cubic	Cubic
Space group	$P\bar{4}3n$ (No. 218)	$F\bar{4}3m$ (No. 216)
a (Å)	10.76781(5)	5.39813(5)
V (Å^3)	1248.48(2)	157.30(1)
Formula weight	583.67	72.72
ρ_{calc} (g cm^{-3})	4.65782(7)	4.60621(13)
μ (mm^{-1})	4.32505(7)	4.94961(14)
Radiation, λ (Å)	0.354246	
Temperature (K)	295.15	
Refinement results		
Goodness of fit, χ^2	1.896	
R_{p}	6.62%	
R_{wp}	8.31%	
R_{exp}	4.38%	
R_I	2.47%	4.43%
Mass %	58.44(4)	Minor

Table S3b: Atomic coordinates and displacement parameters (U_{iso}, Å^2) of colusite phase for sample BM-873K)

Site	Wyck.	x	y	z	Occ.	U_{iso}
V2a	2a	0	0	0	1	0.0155(4)
Sn6c	6c	0.25	0.5	0	1	0.0197(6)
Cu6d	6d	0.25	0	0.5	1	0.0155(4)
Cu8e	8e	0.2533(5)	0.2533(5)	0.2533(5)	1	0.0155(4)
Cu12f	12f	0.2536(3)	0	0	1	0.0155(4)
S8e	8e	0.1287(11)	0.1287(11)	0.1287(11)	1	0.0109(6)
S24i	24i	0.3790(3)	0.3672(3)	0.1225(10)	1	0.0109(6)
Cu24i	24i	0	0.25	0.25	0.0057(18)	0.0155(4)

Table S3c: Atomic coordinates and displacement parameters (U_{iso}, Å^2) of sphalerite-type phase for sample BM-873K

Site	Wyck.	x	y	z	Occ.	U_{iso}
M[a]	4a	0	0	0	1	0.0164(5)
S	4c	0.25	0.25	0.25	1	0.0127(15)

[a]Mixed occupancy: Cu 0.755(19), Sn 0.245(19)

Table S3d: Refined cell parameters of bonattite ($CuSO_4 \cdot 3\,H_2O$) phase for sample BM-873K

	Space group	a (Å)	b (Å)	c (Å)	β (°)	Volume (Å^3)
bonattite	Cc	5.609(3)	13.071(8)	7.352(4)	97.19(5)	534.8(5)

Table S4a: Crystal data and structure refinement for BM-1023K sample

Parameter	**Cu-V-Sn-S (Colu)**	**Cu-Sn-S (sph)**
Crystal system	Cubic	Cubic
Space group	$P\bar{4}3n$ (No. 218)	$F\bar{4}3m$ (No. 216)
a (Å)	10.76920(11)	5.40230(5)
V (Å^3)	1248.97(4)	157.67(1)
Formula weight	582.53	77.67
ρ_{calc} (g cm^{-3})	4.64695(14)	4.90799(15)
μ (mm^{-1})	4.31753(13)	6.6162(2)
Radiation, λ (Å)	0.354246	
Temperature (K)	293(2)	
Refinement results		
Goodness of fit, χ^2	2.26	
R_{p}	8.09%	
R_{wp}	10.08%	
R_{exp}	4.46%	
R_I (Colu phase)	1.95%	
R_I (sph phase)	4.50%	

Table S4b: Atomic coordinates and displacement parameters (U_{iso}, Å^2) of colusite phase BM-1023K

Site	Wyck.	x	y	z	Occ.	U_{iso}
V2a	2a	0	0	0	1	0.0155(5)
Sn6c	6c	0.25	0.5	0	1	0.0191(8)
Cu6d	6d	0.25	0	0.5	1	0.0155(5)
Cu8e	8e	0.2546(5)	0.2546(5)	0.2546(5)	1	0.0155(5)
Cu12f	12f	0.2534(4)	0	0	1	0.0155(5)
S8e	8e	0.1289(13)	0.1289(13)	0.1289(13)	1	0.0105(8)
S24i	24i	0.3789(4)	0.3681(4)	0.1212(11)	1	0.0105(8)
Cu24i	24i	0	0.25	0.25	0.002(2)	0.0155(5)

Table S4c: Atomic coordinates and displacement parameters (U_{iso}, Å^2) for Cu-Sn-S sphalerite-type phase BM-1023K

Site	Wyck.	x	y	z	Occ.	U_{iso}
M[a]	4a	0	0	0	1	0.0203(5)
S	4c	0.25	0.25	0.25	1	0.0080(10)

[a]Mixed occupancy: Cu 0.621(17), Sn 0.379(17)

Table S4d: Refined cell parameters of bonattite ($CuSO_4 \cdot 3\,H_2O$) and chalcanthite ($CuSO_4 \cdot 5\,H_2O$) phases for sample BM-1023K.

	Bonattite	**Chalcanthite**
S.G.	Cc	$P\overline{1}$
a (Å)	5.609(3)	6.122(1)
b (Å)	13.071(8)	10.732(1)
c (Å)	7.352(4)	5.961(1)
α (°)	90	82.35(1)
β (°)	97.19(5)	107.28(1)
γ (°)	90	102.60(1)
V (Å^3)	534.8(5)	364.0(1)